# Multiphysics Modeling of the Atrial Systole under Standard Ablation Strategies

Julia M. Hörmann,[1] Cristóbal Bertoglio ⦿,[1,3] Andreas Nagler,[1] Martin R. Pfaller,[1] Felix Bourier,[2] Martin Hadamitzky,[2] Isabel Deisenhofer,[2] and Wolfgang A. Wall[1]

[1]Institute for Computational Mechanics, Technical University of Munich, Boltzmannstr. 15, 85748 Garching b. München, Germany; [2]Deutsches Herzzentrum München, Technical University of Munich, Lazarettstr. 36, 80636 Munich, Germany; and [3]Numerical Biomedicine Lab, Center for Mathematical Modeling, Universidad de Chile, Beauchef 851, Santiago, Chile

**Abstract**—The aim of this study was to develop a computational framework to compare the impact of standard ablation concepts on the mechanical performance of the atria, since different line combinations cannot be applied in practice to the same patient. For this purpose, we coupled electro-mechano-hemodynamic mathematical models based on biophysical principles and simulate the contractile performance of the atria. We computed systolic pressures and volumes in two patient-specific atrial geometries (one of normal size and one hypertrophied) with various ablation concepts. We found that our computational model is able to detect the differences in the left atrial contractility and ejection fraction for various electrical activation sequences resulting from different ablation line combinations. We show that multiphysics modeling has the potential to quantify the hemodynamic performance of left atria for different ablation lines, which could be used as additional pre-operative clinical information for the choice of the ablation concept in the future.

**Keywords**—Catheter ablation, Electro-fluid-tissue biophysics, Mathematical modeling, Computational simulations.

## ABBREVIATIONS

| | |
|---|---|
| LA | Left atrium |
| AL | Anterior line |
| AF | Atrial fibrillation |
| BL | Posterior box set |
| CFAE | Complex fractionated atrial electrograms on both sites |
| CFAE-ant | CFAE on the anterior site |
| CFAE-post | CFAE on the posterior site |
| CMRT | Cardiac magnetic resonance tomography |
| CT | Computed tomography |
| EF | Ejection fraction |
| MIL | Mitral isthmus line |
| PV | Pulmonary vein |
| PVI | PV isolation |
| RL | Roofline |
| WACA | Wide area circumferential ablation |

Address correspondence to Cristóbal Bertoglio, Numerical Biomedicine Lab, Center for Mathematical Modeling, Universidad de Chile, Beauchef 851, Santiago, Chile. Electronic mail: cbertoglio@dim.uchile.cl

## INTRODUCTION

AF is the most common sustained cardiac arrhythmia and a leading cause of thromboembolic cerebral insults.[20] In general, AF is described by chaotic electrical waves traveling along myocardial tissue, preventing a regular contraction of the atrium.[19] Patients suffering from AF are additionally exposed to an increased risk of stroke, cardiac failure, and mortality.[42] Due to the limited success rate of drug therapy[9] interventional treatments in terms of radiofrequency catheter ablation are the methods of choice.

PVI is the standard ablation approach of paroxysmal AF.[3] However, in the case of persistent AF, several additional ablation concepts are established, comprising ablation of CFAE, ablation of atrial lines[40] or rotor-ablation.[18,36] By now the effect of these ablation concepts on atrial contractility and atrial EF remains unclear.

Atrial contribution to ventricular filling is known to be as 10–40% and increases with age.[2] Hence, choosing the most suitable ablation concept also considering the hemodynamic performance of the left atrium after the procedure may improve the postoperative cardiac performance, especially in older patients.[24]

In clinical studies, the effect of different ablation strategies can hardly be examined without having patient-dependent conditions. Moreover, in clinical trials only a single ablation concept can be applied in one patient and thus a direct comparison is not possible.

In the last decade various simulation approaches were reported examining the impact of different ablation techniques on the excitation sequence and during fibrillation in atrial models[26,32,33] in order to investigate if AF terminates under the setup of different AF initiation[32] and incomplete ablation lines.[33] To the best of our knowledge, the only work considering electromechanical coupling (without hemodynamic effects) in the atria is the one of.[1]

However, none of these works analyzed the impact of the ablation concepts on the atrial mechanics and its contribution to ventricular filling, since the mechanics of the tissue and the fluid were not taking into account. Hence, the aim of the present study is to fill this gap and to assess the ablation approaches with regard not only to the electrical activation sequence of the atria but in particular to the activation triggered contraction and hemodynamic performance.

For this purpose, we present a computational model bridging all three main physical phenomena: the electrophysiological wave propagation, myocardial contraction and blood pressure development. We simulated the atrial function for two different patient-specific geometries, non-pathological, and dilated, to investigate the influence of the different ablation concepts on the activation sequences and mechanical performance (in terms of EF).

## MATERIALS AND METHODS

The biophysical model used within this study included patient-specific geometries with anatomical fiber orientation and was composed as coupled electrophysiological, mechanical and hemodynamic models. In each of these coupled models the ablation lines were defined through different material properties in comparison to healthy tissue.

### Starting Image Data

We developed biophysical computational models from two patients: Model 1 was obtained from a cardiac CT with a resolution of $0.4 \times 0.4 \times 0.8$ mm$^3$ from a 71-old individual without known cardiac pathological findings. Model 2 was obtained from CMRT with a resolution of $1.4 \times 1.4 \times 1.5$ mm$^3$ from dilated atria of a 62-old individual with paroxysmal AF. We used different image data to verify that both medical imaging techniques, CT and CMRT, can be processed with our methodology to simulate, with a patient-specific geometry, the performance of the atria.
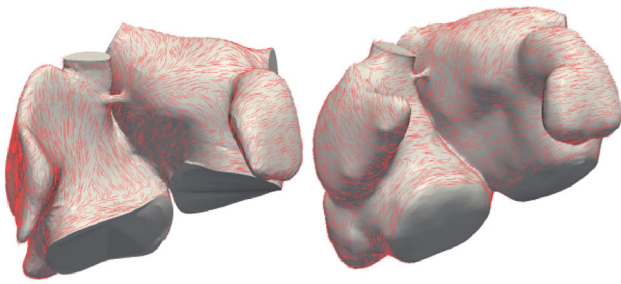
### Geometrical and Fiber Models

Starting from the respective images of Models 1 and 2, a surface representation of both atria was generated using the software Mimics (Materialise, Leuven, Belgium). First, the lumina of both atria were segmented manually, so that the endocardial surfaces of the atrial wall are obtained. Then, we generated the epicardium by extruding the luminal surfaces 2 mm. Finally, a volume mesh was created using Gmsh,[17] with a maximal mesh element size of 0.9 mm, resulting in 370,000 and 510,000 linear tetrahedral elements for Models 1 and 2, respectively. The size of 0.9 mm was chosen to ensure that the thin atrial wall has in every case at least two elements throughout the wall thickness. The segmented geometries are presented in Fig. 1, including a visualization of the ablation lines.

To both geometries, local fiber directions were assigned semi-automatically using reported knowledge of atrial fiber structure[21] and harmonic interpolation techniques[31] see Fig. 2.

We integrated the main fiber bundles in the right and left atrium (crista terminalis, pectinate muscles, circumferential vestibule fibers and Bachmann bundle), which run through the whole atrial wall thickness. In the remaining part of the tissue, we defined different
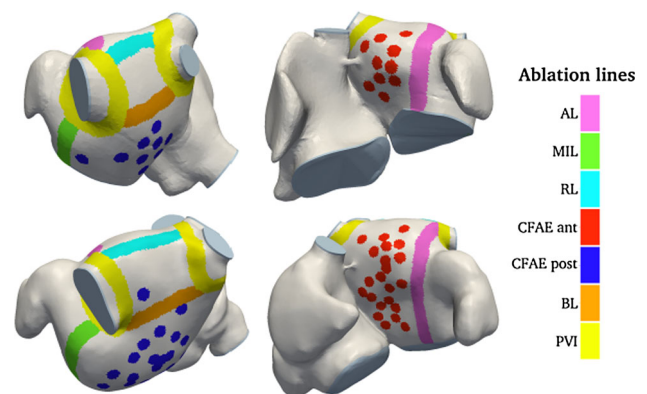


FIGURE 1. Segmented biatrial geometries for Model 1 (top) and Model 2 (bottom) with the different ablation lesions PVI, AL, MIL, CFAE, RL and BL. WACA is not shown in this figure for the sake of clarity, since it consists in a "wider PVI" lesion. Its spatial extension can be appreciated through the electrically inactive area in Fig. 4c.

**FIGURE 2.** Assigned fiber orientation for Model 1 (left) and Model 2 (right).

fiber directions on each epi- and endocardial surface of each section. The fibers were interpolated into the whole thickness using a Poisson operator.

## Geometrical Model of Ablation Patterns

We included following ablation lesions in both models: PVI, WACA, AL, MIL, RL, BL, and CFAE, CFAE-ant, CFAE-post. All ablation lines were placed on a three-dimensional representation of the epicardial surface, using the software 3-matic (Materialise, Leuven, Belgium). This virtual ablation procedure was performed by a trained clinical electrophysiologist, based on the individual anatomy of the two atrial geometries, and hence the ablations lines are comparable with the ones during a real surgical procedure. The ablation lines had an averaged width of 5 mm and penetrated the atrial wall entirely to the endocardial surface. We assume an ablation procedure without imperfections, such as gaps and discontinuities, since the focus of this study was the impact of a successful ablation procedure on global atrial performance.

We integrated the described ablation lines as different sub-regions of the atrial domain for both models. The performed computational simulations include these specific ablation lines and all medically feasible combinations of them (denoted with a " + ").

## Electrophysiological Model

We assumed that all ablation concepts lead to a termination of atrial fibrillation, restoring normal sinus rhythm, meaning an activation current was applied solely at the sinus node.

The propagation of the electrophysiological wave was computed using the monodomain equations for the transmembrane potential and gating membrane variable[14] and the Bueno-Orovio cellular model.[8] The model parameters of the cellular model were adapted to reproduce atrial excitation properties, according to Weber et al.[41] The diffusivity was assumed transverse isotropic with a diffusivity of 0.6 mm$^2$/ms in fiber direction and 0.06 mm$^2$/ms perpendicular to it. These

values were chosen to obtain a physiological propagation velocity and activation time for the standard atrial geometry (Model 1) without ablation lines.[22] The same diffusivity values were then used for the dilated geometry (Model 2), naturally leading to a larger activation time. We modeled the ablated necrotic tissue as a perfect isolator, i.e. with zero diffusivity. This implies that the necrotic tissue is no longer electrically activated and hence it does not contract.

Concerning the numerical methods, the spatial semi-discretization was performed *via* a linear continuous Galerkin approach, with the ionic currents computed at the element center. The time semi-discretization is fully implicit, meaning that a Newton approach has to be applied in order to solve for the nonlinearity of the reaction term. This allows working with a time step of 0.1 ms, compared with the time need for the activation in the cellular model of 1 ms.

The activation wave is plotted in Fig. 3 for both models without any ablation and with ablation concept PVI + AL + BL.

## Mechanical Model

The mechanical behavior of myocardial tissue of both atria is characterized by both its passive stiffness and its ability to contract, triggered by the electrical signal. The tissue mechanical model is based on the nonlinear elastodynamic equations, with the passive part represented as a nearly incompressible Mooney–Rivlin material, plus an active stress component.[11] We used a simplified version of an excitation–contraction model,[5] retaining three parameters: the maximal active tension, the myosin attachment and detachment rate. The activation function for the Bestel model at each structural element is equal to 1 once the element center is electrically activated. A similar coupling strategy was performed by Corrado et al.[15] through a scaled electrical potential obtaining realistic electromechanical physiological response.

The maximal active tension (or *contractility*) was fixed as 10$^5$ Pa for both Models 1 and 2, which led to an EF of 21 and 16% in Model 1 and Model 2, respectively. Thus in the non-dilated atria we obtained an ejected volume which corresponds to an atrial contribution to the end-diastolic ventricular volume of 38% of Model 1 as reported in a clinical study.[2] The myosin attachment and detachment rate was set to 20 and $-30$ s$^{-1}$, respectively, in order to assure physiological pressures. At each spatial point the model independently converts the electrical activation into an active tension, which was applied in the local fiber direction. We remark that, since the ablated tissue was not activated, it did not contract, as we assumed that contraction is solely induced by the electrical signal as
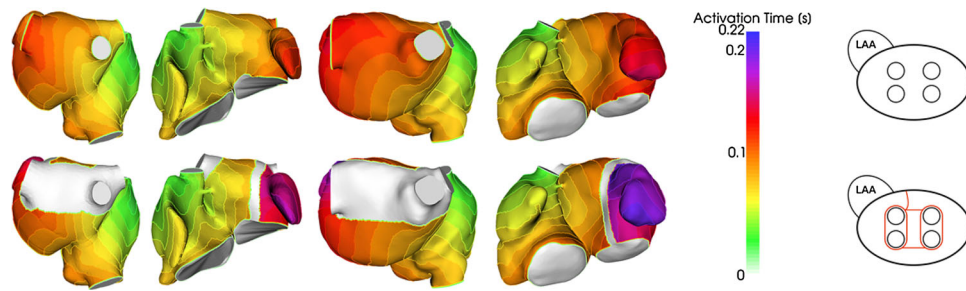
**FIGURE 3.** Isochrones of the propagation wave for Model 1 (left) and Model 2 (right) without (top) and with (bottom) ablation concepts including PVI + AL + BL. We include a scheme of the LA and the LA appendage (LAA) with the ablation concept (red) for the sake of clarity.

routinely observed in clinical practice, i.e. no stretch-activated channels are modeled. Moreover, we considered the interaction with the pericardium and external tissue by including an elastic model in the surface normal direction on the epicardium.[29] As the title of the manuscript suggests, since we are interested in the systolic performance of the atria only, the ventricle was considered as a passive stiffness on the heart base.

The numerical solution of the solid model was performed using linear continuous finite elements for the space-semidiscretization, while the time semi-discretization is backward Euler with implicit treatment of the elastic forces.

## Hemodynamic Model

The interaction of the atrial wall with the blood was considered through strongly coupling a Windkessel model with the elastic myocardial wall. A Windkessel is a physically-based mathematical representation of the relation between mean pressures and flow rates in a certain geometry.[37] In our case, we assigned a single pressure degree-of-freedom per cardiac chamber. The left ventricle was modeled as constant capacitance of $1.88 \times 10^{-8}$ m$^3$/Pa acting as a passive elastic component. We used the same ventricular hemodynamics for both models, Model 1 and Model 2, since we assumed that the ventricles were not influenced by atrial fibrillation and the resulting dilation of the atria. The mitral valve was modeled as flow resistance between the atrial and ventricular chambers, which took high values when the ventricular pressure was higher than the atrial pressure (hence restricting the leakage into the atria) and low values when the atrial pressure exceeds the ventricular one, allowing blood only to flow in atrial-ventricular direction. This results in variations of the atrial chamber pressure between 8 and 15 mmHg for Model 1 and 8 and 18 mmHg for Model 2 without ablated tissue, for atrial diastole and systole, respectively.

In our model we assumed that no backflow in the pulmonary veins exists, thus all blood leaving the atrium is flowing into the ventricle.

Both solid and hemodynamic models were coupled implicitly in time, leading to a single system of equations, which was solved iteratively using block-LU preconditioner allowing an efficient algebraic treatment of the solid-Windkessel coupling.

## RESULTS

### Perfect Ablation Lines

To illustrate the versatility of the multiphysics modeling framework, we compare 15 different ablation concepts representing current clinical ablation standards on the two bi-atrial models presented above. We analyzed the simulation results in terms of activation sequence and duration, volume over time and the correlation of the amount of inactive and ablated tissue with EF.

Figure 3 shows the activation map for Model 1 without any ablation lines (top left). The activation map correspond well with an experimental gained activation map,[16] and the activation times lay in the same range as atria in clinical surgery.[28] For Model 2 the activation pattern is similar, besides the fact that the overall activation takes longer. In Model 1 the activation of the complete atria takes around 120 ms and in Model 2 around 150 ms.

Figure 4 shows isochrones of the propagation wave of Model 1 with the simulated sinus rhythm and different ablation lesions, while Fig. 5 presents the atrial time–volume curves. Circumferential PVI does not significantly alter the excitation sequence in the left atrium, since only the orifices of the PVs are not activated anymore (see Figs. 4a and 4b). The WACA ablation procedure disables a larger amount of contractile tissue compared to standard PVI, which has a significant impact on maximal atrial output (see Table 1), although the activation pattern is not altered
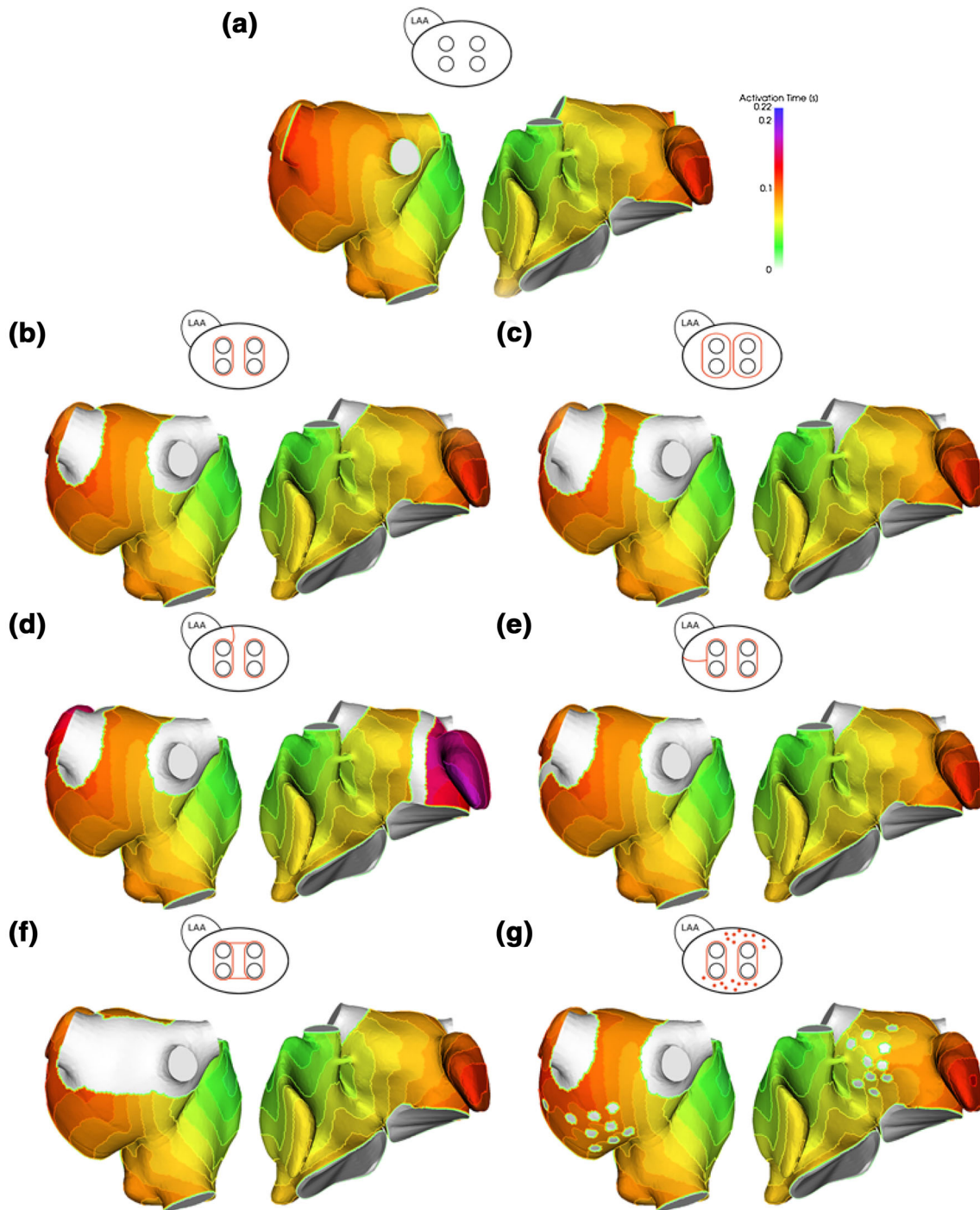
**FIGURE 4.** Isochrones of the propagation wave in sinus rhythm for Model 1 without ablation and with generic ablation lesions. A schematic representation of the ablation lesions is given at the top of each model, which shows the left atrium with the left atrial appendage (LAA) and the four pulmonary veins (circles) from an epicardial latero-dorsal view. The red lines represent the ablation lesions. (a) Activation without ablation lesions; (b) PVI; (c) WACA procedure; (d) PVI + AL; (e) PVI + MIL; (f) PVI +BL; (g) PVI + CFAE ablation.

(see Fig. 4c). A considerably different activation pattern is observable when comparing PVI + AL and PVI + MIL. The combination PVI + MIL does not alter the excitation sequence compared to only PVI, whereas PVI + AL has a significant impact. AL blocks the activation on the anterior side of the left atrium. The left appendage is thus only activated from the posterior side, resulting in a significant increase in
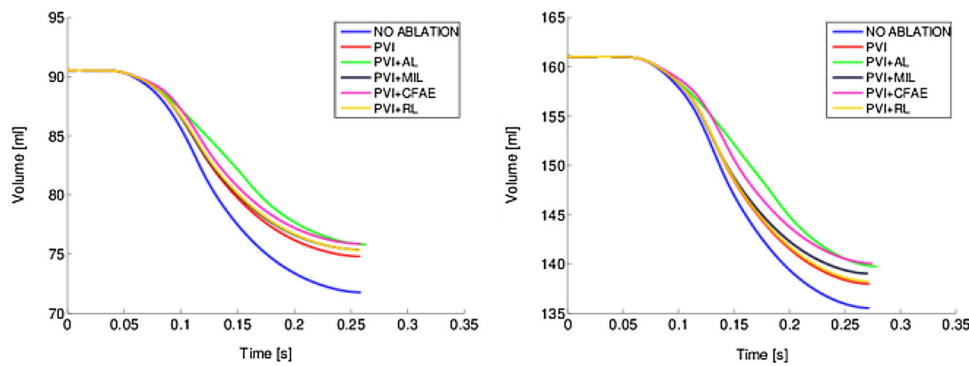
**FIGURE 5.** Computed volume curve for Model 1 (left) and Model 2 (right). The curves end at their peaks systole, i.e. maximal contraction of the atria. Shown in the plots are the volume curves for no ablation (blue), PVI (red), PVI + AL (green), PVI + MIL (black), PVI + CFAE (purple) and PVI + RL (yellow).

activation time (around 50 ms in both models) (see Fig. 4d and 4e). The ablation PVI + BL does not significantly alter the excitation sequence but inactivates a large portion of left atrial tissue on the roof (see Fig. 4f and Table 1). The ablation lesion PVI + C-FAE leads to small inhomogeneities in the activation on the anterior and posterior side and a slight increase in activation time (see Fig. 4g). For Model 2, the results of the activation sequence were similar apart from the natural prolongation of the activation time due to the increased size of the atria.

Figure 5 shows the computed time-volume curves of the left atrium until left atrial peak systole for both Models 1 and 2 with the basic ablation line combinations. The plots show that for all ablation lines the time from the onset of contraction to peak systole are identical except for the combination PVI + AL. Additionally to the already stated delay at peak systole for PVI + AL, the descent of the volume curve is less steep, i.e. in comparison to other ablation lines the ejected blood volume is at all time points lower. These observations can be seen in the volume curves for both Model 1 and Model 2.

Table 1 summarizes the results for all ablation approaches in terms of the change (Δ) in EF due to ablation lesions was compared to the baseline model without ablation and a healthy sinus rhythm.

Figure 6 depicts the results for all ablation concepts ordered by ΔEF. It shows that the more extensive the ablation approach, thus electrically isolating more tissue, the greater is the reduction of left atrial output. In both models the ablation pattern including AL inactivated a larger portion of tissue and decreased LA EF more than the combination with MIL.

In Fig. 7 the amounts of ablated tissue and inactive tissue are plotted against ΔEF. Model 1 shows a strong correlation ($R^2 = 0.98$) between inactive tissue and ΔEF and a weaker correlation ($R^2 = 0.75$) between ablated tissue and ΔEF. The correlations for Model 2 show similar behavior for inactive tissue and ΔEF ($R^2 = 0.85$), and ablated tissue and ΔEF ($R^2 = 0.88$).

## Imperfect Ablation Lines

To study the effect of imperfect ablation lines, we performed additional simulations with gaps at different locations in the AL and MIL.

In the AL we included gaps in the upper part, in the middle part and in the lower part of the line and in the MIL we included a gap in the middle of the line (see Fig. 8). Figure 9 shows the activation pattern of the pulmonary vein isolation (PVI) and the PVI + AL ablation concept in comparison to a PVI + AL ablation with gaps on different locations. Figure 10 shows the activation pattern of the ablation concepts PVI, PVI + MIL without a gap and PVI + MIL with a gap. The gaps have an average thickness of 3 mm and go through the entire thickness of the wall. They are modeled as healthy tissue. A complete AL slows the activation of the LAA significantly, while a gap in the line reduces the activation time to a certain level, depending on the location of the gap. The gap in the middle part of the AL reduces the activation time of the LAA the most; the gap in the upper part of the AL reduces the least. This behavior is also visible in the atrial output curves (see Figs. 11 (left) and 12 (left)). The volume curve for the PVI + AL ablation with a gap in the middle part is steeper than the curve of the ablation with a continuous AL. A gap in the MIL does not significantly alter the activation pattern, since the MIL itself does not change the activation pattern. However, an impact on the ejection fraction is visible. Since more contractile tissue exists, the atrial output is bigger when including a gap in the MIL (see Figs. 11 (right) and 12 (right)). The results obtained with Model 1 are analogous as with Model 2.

TABLE 1. Ejection fraction (EF) of left atria with different ablation concepts for Model 1 and Model 2.

| Ablation lines | Max. atrial output (ml) | EF (%) | ΔEF pp | Ablated tissue (%) | Inactive tissue (%) |
|---|---|---|---|---|---|
| **Model 1** | | | | | |
| No ablation | 18.7 | 20.68 | 0 | 0 | 0 |
| PVI | 15.7 | 17.31 | 3.37 | 10.0 | 14.7 |
| PVI + AL | 14.6 | 16.20 | 4.48 | 14.3 | 19.0 |
| PVI + MIL | 15.1 | 16.69 | 3.99 | 12.1 | 16.9 |
| PVI + CFAE | 14.6 | 16.13 | 4.54 | 13.9 | 18.6 |
| PVI + BL | 13.6 | 15.02 | 5.66 | 13.5 | 21.7 |
| PVI + RL | 15.1 | 16.72 | 3.96 | 11.8 | 16.6 |
| PVI + CFAE posterior | 15.1 | 16.71 | 3.97 | 11.6 | 16.3 |
| PVI + CFAE anterior | 15.1 | 16.74 | 3.94 | 12.2 | 17.0 |
| PVI + AL + RL | 14.1 | 15.63 | 5.05 | 16.2 | 20.9 |
| PVI + MIL + RL | 14.5 | 16.08 | 4.60 | 14.0 | 18.8 |
| PVI + AL + BL | 12.7 | 14.02 | 6.66 | 17.9 | 26.0 |
| PVI + MIL + BL | 13.5 | 14.95 | 5.73 | 15.7 | 23.9 |
| PVI + AL + CFAE + RL | 13.1 | 14.44 | 6.24 | 20.1 | 24.8 |
| PVI + MIL + CFAE + RL | 13.5 | 14.95 | 5.73 | 17.9 | 22.7 |
| WACA | 13.8 | 15.24 | 5.44 | 13.0 | 21.6 |
| **Model 2** | | | | | |
| No ablation | 25.4 | 15.77 | 0 | 0 | 0 |
| PVI | 22.9 | 14.24 | 1.53 | 7.9 | 12.7 |
| PVI + AL | 21.1 | 13.14 | 2.63 | 11.0 | 15.8 |
| PVI + MIL | 21.9 | 13.59 | 2.18 | 9.4 | 14.2 |
| PVI + CFAE | 20.8 | 12.95 | 2.82 | 13.3 | 18.1 |
| PVI + BL | 21.4 | 13.30 | 2.47 | 10.8 | 19.6 |
| PVI + RL | 22.7 | 14.08 | 1.69 | 9.4 | 14.1 |
| PVI + CFAE posterior | 21.7 | 13.46 | 2.31 | 10.4 | 15.2 |
| PVI + CFAE anterior | 22.1 | 13.74 | 2.03 | 10.9 | 15.6 |
| PVI + AL + RL | 20.9 | 12.97 | 2.80 | 12.5 | 17.2 |
| PVI + MIL + RL | 21.6 | 13.42 | 2.34 | 10.8 | 15.6 |
| PVI + AL + BL | 19.6 | 12.19 | 3.58 | 13.9 | 22.7 |
| PVI + MIL + BL | 20.3 | 12.63 | 3.14 | 12.2 | 21.1 |
| PVI + AL + CFAE + RL | 18.8 | 11.71 | 4.06 | 17.9 | 22.6 |
| PVI + MIL + CFAE + RL | 19.6 | 12.17 | 3.60 | 16.2 | 21.0 |
| WACA | 21.6 | 13.45 | 2.31 | 8.9 | 17.1 |

*pp* percentage points.

### Reduced Conduction Velocity

In diseased atria it may appear that the conduction velocity is reduced due to, for example, the presence of fibrosis. To investigate the influence of a reduced conduction velocity on the contractility of the left atria we performed additional simulations with different diffusion coefficients. We apply a homogeneous reduction of the diffusion coefficient in all atrial tissue, see e.g., Ref. 25 for taking into account uniform gap junction remodeling. As there exist many types of atrial remodeling,[35] we studied three different reductions of the diffusion coefficient, i.e. 75, 50, and 25%. Figure 13 shows the activation map for Model 1 for the ablation concepts PVI, PVI + AL, and PVI + MIL for the different diffusion coefficients. Decreasing the diffusion coefficient leads to a prolongation of the activation time, which is more clearly visible in the ablation strategy PVI + AL (Fig. 13 (middle row)). In Fig. 14 the volume over time is plotted for the ablation concept PVI + AL for different diffusion coefficients

until the moment of maximal contraction. One can see that the time of maximal contraction is delayed, additionally also the minimal volume is bigger. Thus with decreasing conduction velocity the ejection fraction decreases too, see Fig. 14 (left). Note that the result with a reduced diffusion coefficient is qualitatively the same as for the result with the larger diffusion coefficient besides the fact that the differences between the ablation concepts are bigger. The detailed results for all diffusivities and ablation lines for both models are summarized in Table 2.

### DISCUSSION

We developed a coupled electro-mechano-hemodynamic model of atria which could be used pre-operatively to gain additional information about atrial function and possible clinical outcomes for several options of radiofrequency ablation. While previous computational models of atrial ablation investigated
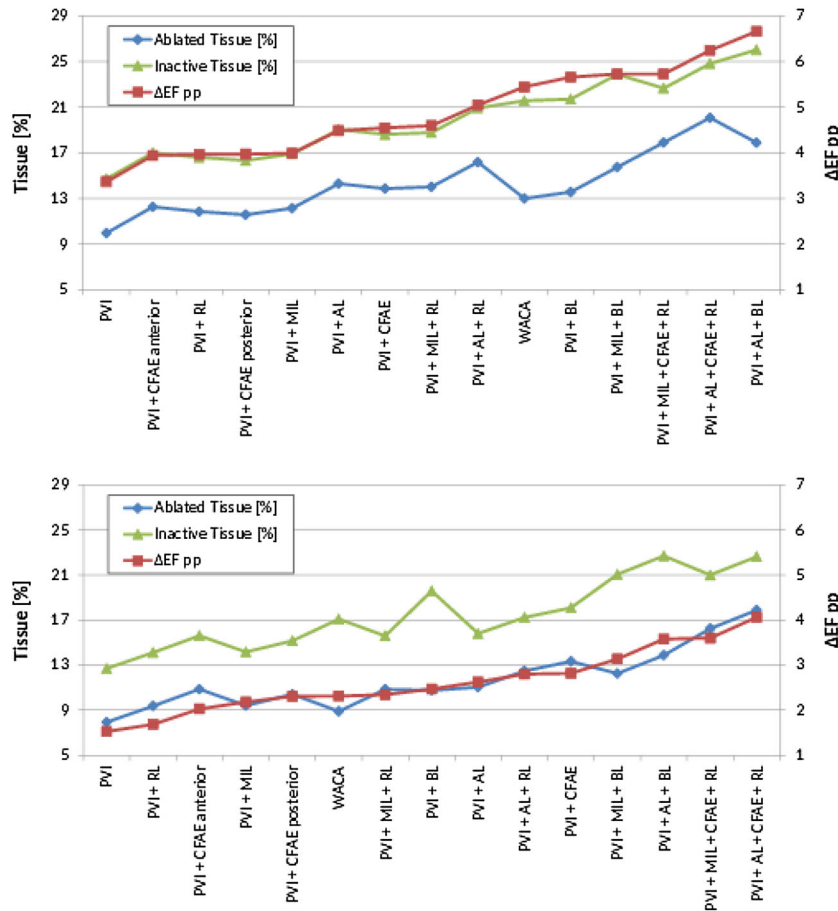
FIGURE 6. Plot for all combinations of ablation lines for Model 1 (top) and Model 2 (bottom) including the change of EF in percentage points (pp), the ablated volume (%) and the inactive volume (%). From left to right the ΔEF increases.
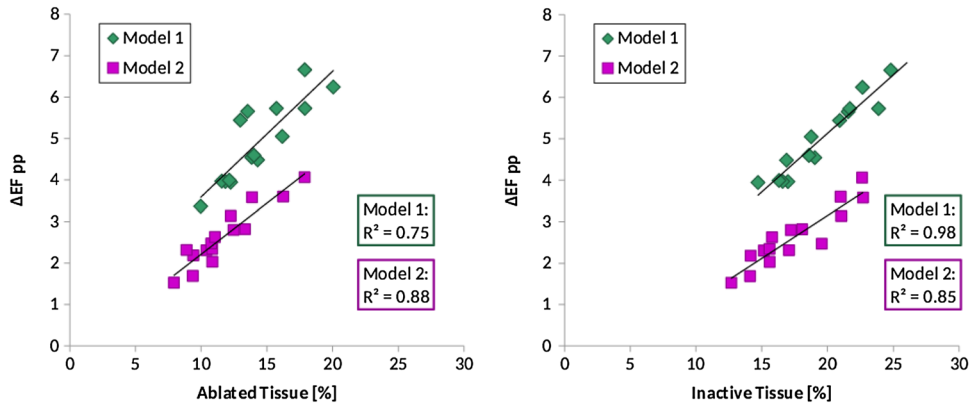


FIGURE 7. Left: plot of ablated tissue (%) against ΔEF percentage points (pp) for Model 1 (green diamond) and Model 2 (purple rectangle) for all combinations of ablation lines. Right: plot of inactive tissue (%) against ΔEF pp for Model 1 (green diamond) and Model 2 (purple rectangle) for all combinations of ablation lines.

electrical propagation, this study focuses on left atrial ejection performance depending on the activation pattern. With our model we calculated the electrical, mechanical and hemodynamic response of two patient-specific atrial geometries with different ablation lines.

This multiphysics coupling allows investigating influences of the electrical activation on the succeeding myocardial contraction and pressure development.

A prolonged activation time for AL ablation is noticeable due to the delayed activation of the left at-
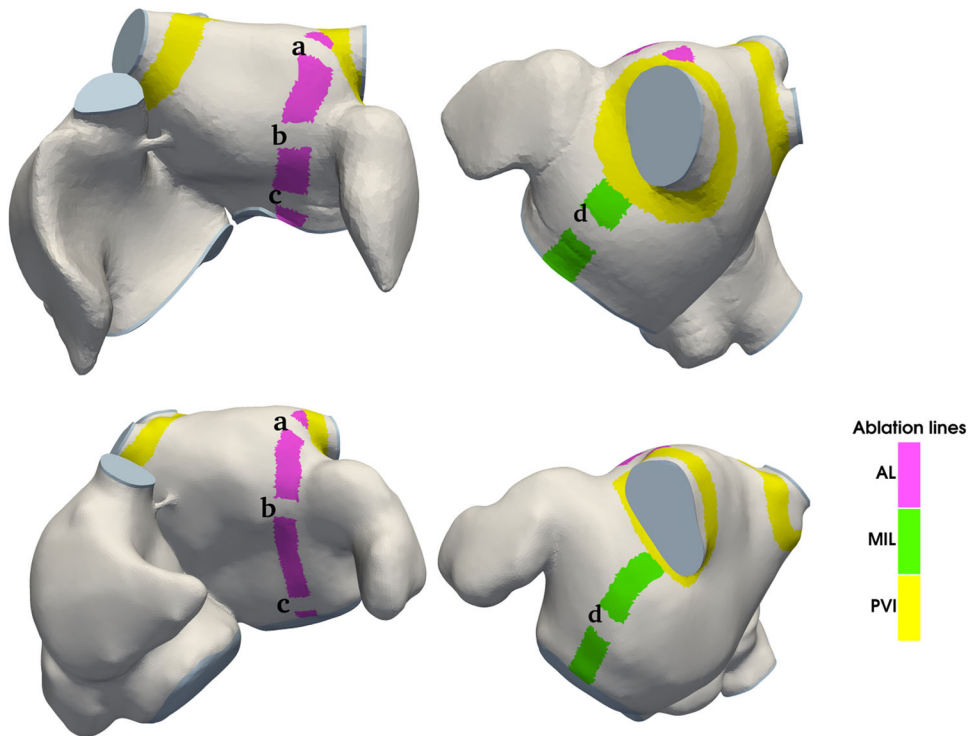
**FIGURE 8.** Gaps in the ablation lines. For Model 1 (top) and Model 2 (bottom) three gaps in the anterior line (a, b, c) and one gap in the mitral isthmus line (d) are tested. The gaps are situated in the upper part of the AL (a); the middle part of the AL (b) and the lower part of the AL (c); and in the mitral isthmus line (d).
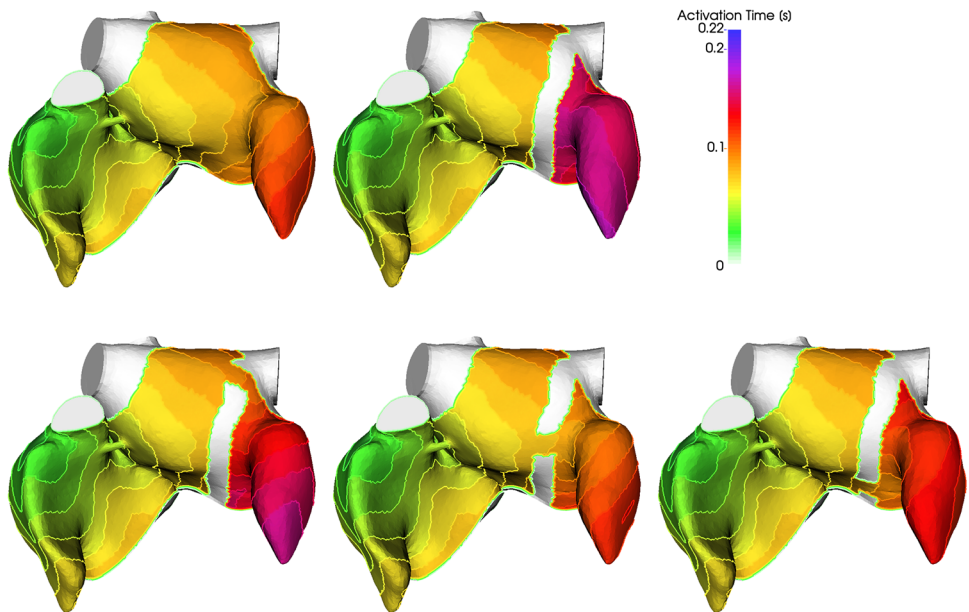


**FIGURE 9.** Activation time for the atria with PVI ablation (top left) and PVI + AL ablation (top right) in comparison with the activation times for the PVI + AL ablation concept with gaps in the AL (bottom). Bottom: gap in the upper part of the AL (left), gap in the middle part of the AL (middle) and gap lower part of the AL (right).

rial appendage (see Fig. 4). This time delay is reflected in a delayed peak systole (see Fig. 5). In the aspect of successful therapy outcome this time delay of peak systole is important since delayed left atrial contraction is known cause of poor left-sided atrio-ventricular coupling. If the time delay is too big it could happen that the start of LA appendage outflow occurs after the beginning of ventricular contraction. This on the other
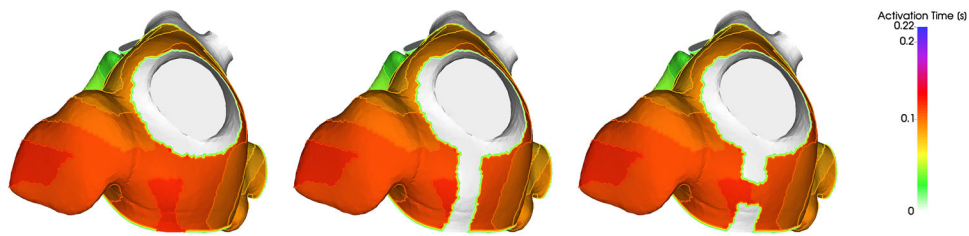
**FIGURE 10.** Activation time for PVI ablation concept (right), PVI + MIL (middle) and PVI + MIL with a gap in the mitral isthmus line.
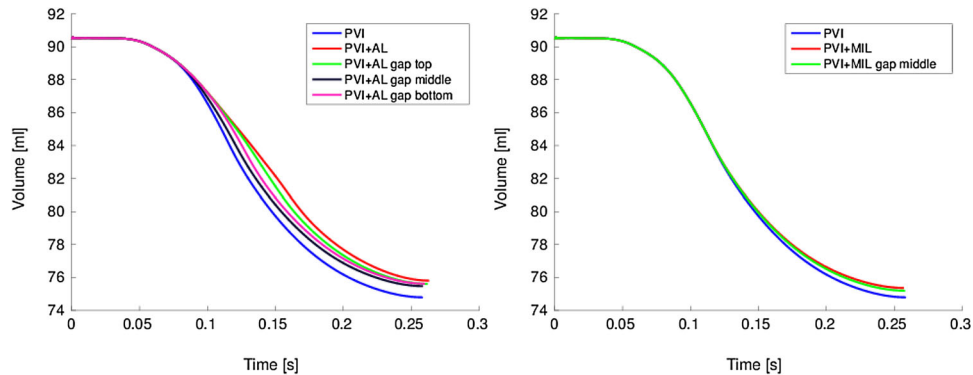


**FIGURE 11.** Volume curves for Model 1 for the AL with gaps (left) and MIL with a gap (right).
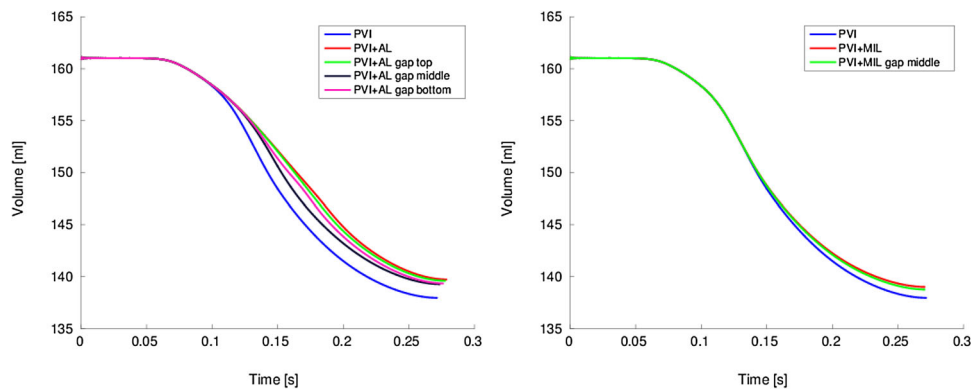


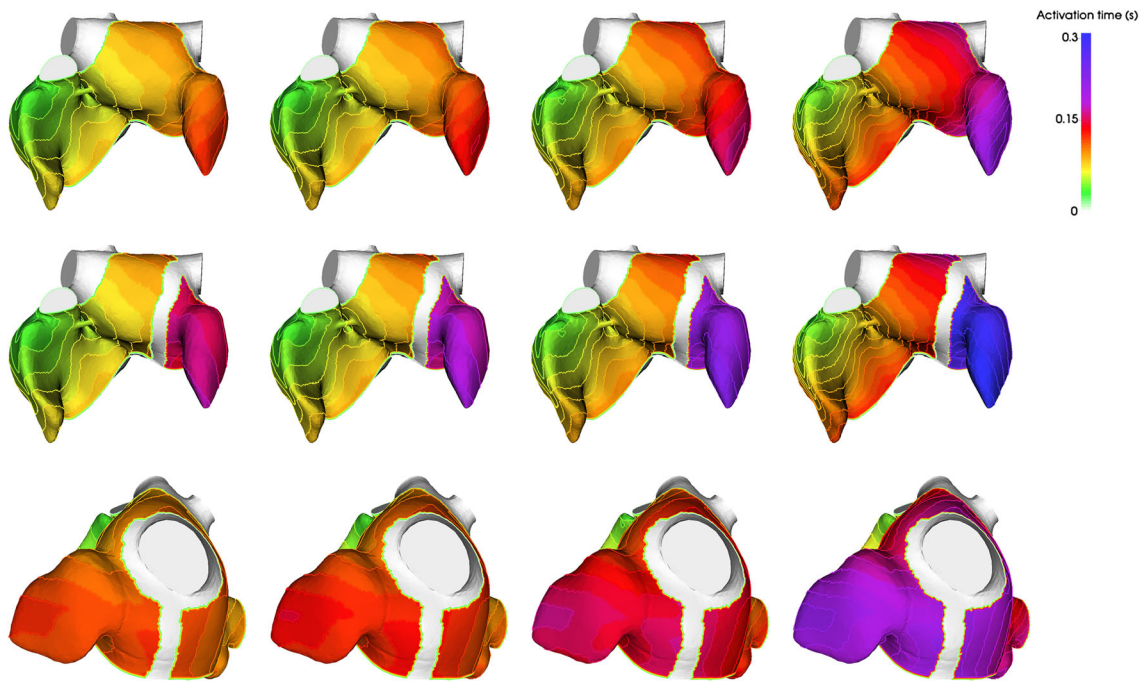**FIGURE 12.** Volume curves for Model 2 for the AL with gaps (left) and MIL with a gap (right).

hand may lead to adversely affected left atrial transport function and to electrical and mechanical remodeling.[34,38,39]

Our model was able to verify that ablation concepts which isolate larger portions of the left atrial tissue lead to a stronger decrease in the active contraction of the atrium. In the non-dilated model the LA EF decrease has as strong correlation with the percentage of inactive tissue, while in the dilated model the correlation is slightly less distinctive.

The results indicate a linear correlation between the change in EF and the amount of inactive tissue (see Fig. 7). In the non-dilated atrium the strong linear correlation of the decrease of EF with the amount of inactive tissue indicates that rather the spatial extension than the location of the ablation line is the key aspect impacting the mechanical performance of the atria after ablation. A recent clinical study[13] based on magnetic resonance imaging, demonstrated the correlation between the extent of scar tissue after radiofrequency ablation and decrease in LA EF, consistent with our findings. The difference between Model 1 and Model 2 in the reduction of EF can be explained by the fixed width of the ablation line used in the simulations. This results in a bigger percentage of ablated tissue in small atria.

Investigating the differences in the atrial mechanical output with simulations of imperfect lines, confirms

**FIGURE 13.** Activation time for Model 1 for the left atria with the diffusivities 0.6, 0.45, 0.3, and 0.15 mm$^2$/ms (form left to right) and the ablation concepts PVI, PVI + AL and PVI + MIL (from top to bottom).
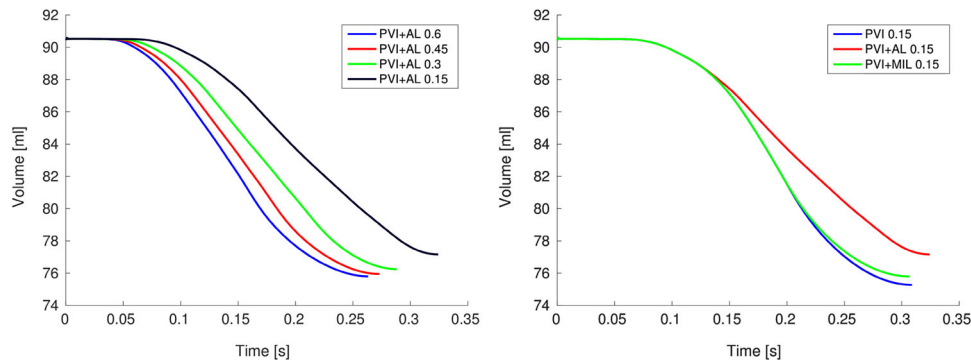


**FIGURE 14.** Volume curves for Model 1 for the PVI + AL for different diffusivity values (left) and for PVI, PVI + AL and PVI + MIL for a diffusivity of 0.15 mm$^2$/ms (right).

that the atrial EF is mainly proportional to the amount of remaining contractile tissue after ablation.

The results in diseased atria are qualitatively the same as in atria with normal conduction velocity. However, in the case of a reduced conduction velocity the contractility of the chamber is also reduced and moreover the differences between the ablation concepts are more relevant. This motivates further studies about the proper choice of the ablation strategy taking also into account mechanical and hemodynamic criteria.

### Clinical Significance

Currently there is no general evidence that favors particular ablation lines.[7,12,23] Impact on the hemo-dynamic performance predicted by multiphysics modeling could be used as additional pre-operative criteria for choosing the ablation concept.

### Limitations and Perspectives

This study considered the three main aspects of the atrial physiology, namely the electrical propagation, the tissue contractility and the hemodynamic feedback. The blood pressure was represented using a lumped parameter model and hence spatial variations of the flow behavior inside each chamber were neglected. Further investigations could analyze the effect of different ablation lines on the flow behavior of the blood in the left atria, the left atrial appendage and the mitral

**TABLE 2.** Ejection fraction (EF) of left atria with different diffusion coefficients for the basic ablation concepts PVI, PVI + AL and PVI + MIL for Model 1 and Model 2.

| Diffusivity (mm$^2$/s) | Ablation lines | Max. atrial output (ml) | EF (%) | $\Delta$ EF pp | Time max. contraction (s) | Time activation (s) |
|---|---|---|---|---|---|---|
| Model 1 | | | | | | |
| 0.6 | No ablation | 18.70 | 20.68 | 0.00 | 0.26 | 0.12 |
| | PVI | 15.66 | 17.31 | 3.36 | 0.26 | 0.12 |
| | PVI + AL | 14.65 | 16.20 | 4.48 | 0.26 | 0.17 |
| | PVI + MIL | 15.09 | 16.69 | 3.99 | 0.26 | 0.12 |
| 0.45 | PVI | 15.60 | 17.25 | 3.43 | 0.27 | 0.14 |
| | PVI + AL | 14.50 | 16.03 | 4.65 | 0.27 | 0.19 |
| | PVI + MIL | 15.04 | 16.63 | 4.05 | 0.27 | 0.14 |
| 0.3 | PVI | 15.49 | 17.12 | 3.55 | 0.28 | 0.16 |
| | PVI + AL | 14.20 | 15.70 | 4.98 | 0.29 | 0.23 |
| | PVI + MIL | 14.94 | 16.51 | 4.17 | 0.28 | 0.16 |
| 0.15 | PVI | 15.18 | 16.78 | 3.90 | 0.31 | 0.21 |
| | PVI + AL | 13.29 | 14.69 | 5.99 | 0.32 | 0.31 |
| | PVI + MIL | 14.65 | 16.20 | 4.48 | 0.31 | 0.21 |
| Model 2 | | | | | | |
| 0.6 | No ablation | 25.36 | 15.77 | 0.00 | 0.27 | 0.15 |
| | PVI | 22.91 | 14.24 | 1.52 | 0.27 | 0.15 |
| | PVI + AL | 21.14 | 13.14 | 2.63 | 0.28 | 0.2 |
| | PVI + MIL | 21.86 | 13.59 | 2.18 | 0.27 | 0.15 |
| 0.45 | PVI | 22.78 | 14.16 | 1.61 | 0.28 | 0.17 |
| | PVI + AL | 20.81 | 12.93 | 2.83 | 0.29 | 0.23 |
| | PVI + MIL | 21.73 | 13.51 | 2.26 | 0.28 | 0.17 |
| 0.3 | PVI | 22.53 | 14.01 | 1.76 | 0.30 | 0.2 |
| | PVI + AL | 20.15 | 12.52 | 3.24 | 0.31 | 0.27 |
| | PVI + MIL | 21.50 | 13.37 | 2.40 | 0.30 | 0.2 |
| 0.15 | PVI | 21.84 | 13.58 | 2.19 | 0.34 | 0.26 |
| | PVI + AL | 18.20 | 11.31 | 4.45 | 0.36 | 0.36 |
| | PVI + MIL | 20.86 | 12.97 | 2.80 | 0.33 | 0.26 |

valve to study possible clot formation for minimizing stroke risk in AF.[42]

Since the focus of this study was to evaluate the hemodynamic performance of the left atria under different ablation concepts where only the geometry was taken patient-specific, all other model parameter were chosen from the literature, what allowed to obtain activation patterns and atrial pressures in a physiological range. However, to use our model for predictive purposes it is necessary to adapt the parameter to patient-specific atrial properties and future work may also include the estimation of constitutive tissue properties using clinical measurements and data assimilation approaches.[4,10,26,27,29,30] In any case, the sensitivity of the model's output to the physical parameters (constitutive constants, fiber directions, wall thickness variability, *etc.*) should be estimated using uncertainty quantification techniques as it was done for example for abdominal aortic aneurysm.[6] An important work has of course to be later carried out in investigating if these uncertainties may influence the clinical decision associated to the model's output.

In this study we did not take into account the role of fibrotic tissue and fibrosis in dilated atria and around ablation lesions. Fibrosis could lead to a slowed propagation of the electrical signal and to different propagation patterns if the distribution of the fibrosis is not homogeneous. Fibrosis would also influence contractile properties of the atria and thus deviating hemodynamic performance is expected.

Additionally, remodeling of the atrial myocytes after long-lasting fibrillation would lead to changes in the electrical and contractile properties of the atria. The impact of atrial myocyte remodeling on the electrophysiology and the mechanical performance of the atria was investigated by Adeniran *et al.*,[1] but without taking into account the effect of ablation lines. In this study, we assumed that after the ablation procedure all remodeling of the myocytes is reversed after some time. And since the focus of this study was in the long-term performance, we did not investigate the hemodynamic performance immediately after the surgical intervention where remodeled atrial myocytes are still present. Investigating the influence of partially remodeled atria could be aspect of further studies.

A further interesting and clinically relevant application of a sophisticated multiphysics framework is to study the effect in the mechanical performance of

incomplete ablation lines, which is known to lead to complicated electrical propagation patterns.

## ACKNOWLEDGMENTS

## CONFLICT OF INTEREST

All authors declare that they have no conflict of interest.

## STATEMENT OF HUMAN STUDIES

All procedures followed were in accordance with the ethical standards of the responsible committee on human experimentation (institutional and national) and with the Helsinki Declaration of 1975, as revised in 2000 (5). Informed consent was obtained from all patients for being included in the study.

## STATEMENT OF ANIMAL STUDIES

No animal studies were carried out by the authors for this article.

## REFERENCES

[1]Adeniran, I., D. H. MacIver, C. J. Garratt, J. Ye, J. C. Hancox, and H. Zhang. Effects of persistent atrial fibrillation-induced electrical remodeling on atrial electro-mechanics—insights from a 3D model of the human atria. *PLoS ONE* 10:e0142397, 2015. doi:10.1371/journal.pone.0142397.

[2]Alhogbani, T., O. Strohm, and M. G. Friedrich. Evaluation of left atrial contraction contribution to left ventricular filling using cardiovascular magnetic resonance. *J. Magn. Reson. Imaging* 37:860–864, 2013. doi:10.1002/jmri.23881.

[3]Arentz, T., R. Weber, G. Bürkle, C. Herrera, T. Blum, J. Stockinger, *et al*. Small or large isolation areas around the pulmonary veins for the treatment of atrial fibrillation? Results from a prospective randomized study. *Circulation* 115:3057–3063, 2007. doi:10.1161/CIRCULATIONAHA.107.690578.

[4]Bertoglio, C., D. Barber, N. Gaddum, I. Valverde, M. Rutten, P. Beerbaum, *et al*. Identification of artery wall stiffness: In vitro validation and in vivo results of a data assimilation procedure applied to a 3D fluid–structure interaction model. *J. Biomech.* 47:1027–1034, 2014. doi:10.1016/j.jbiomech.2013.12.029.

[5]Bestel, J., F. Clément, M. Sorine. A biomechanical model of muscle contraction. In: Med. Image Comput. Comput.-Assist. Interv.—MICCAI 2001, edited by W. J. Niessen and M. A. Viergever. Springer: Berlin, 2001, pp. 1159–1161.

[6]Biehler, J., M. W. Gee, and W. A. Wall. Towards efficient uncertainty quantification in complex and large-scale biomechanical problems based on a Bayesian multi-fidelity scheme. *Biomech. Model. Mechanobiol.* 14:489–513, 2014. doi:10.1007/s10237-014-0618-0.

[7]Brooks, A. G., M. K. Stiles, J. Laborderie, D. H. Lau, P. Kuklik, N. J. Shipp, *et al*. Outcomes of long-standing persistent atrial fibrillation ablation: a systematic review. *Heart Rhythm* 7:835–846, 2010. doi:10.1016/j.hrthm.2010.01.017.

[8]Bueno-Orovio, A., E. M. Cherry, and F. H. Fenton. Minimal model for human ventricular action potentials in tissue. *J. Theor. Biol.* 253:544–560, 2008. doi:10.1016/j.jtbi.2008.03.029.

[9]Calkins, H., K. H. Kuck, R. Cappato, J. Brugada, A. J. Camm, S.-A. Chen, *et al*. 2012 HRS/EHRA/ECAS expert consensus statement on catheter and surgical ablation of atrial fibrillation: recommendations for patient selection, procedural techniques, patient management and follow-up, definitions, endpoints, and research trial design. *Heart Rhythm* 9:632–696, 2012. doi:10.1016/j.hrthm.2011.12.016.

[10]Chabiniok, R., P. Moreau, P.-F. Lesault, A. Rahmouni, J.-F. Deux, and D. Chapelle. Estimation of tissue contractility from cardiac cine-MRI using a biomechanical heart model. *Biomech. Model. Mechanobiol.* 11:609–630, 2011. doi:10.1007/s10237-011-0337-8.

[11]Chapelle, D., P. Le Tallec, P. Moreau, and M. Sorine. Energy-preserving muscle tissue model: formulation and compatible discretizations. *Int. J. Multiscale Comput. Eng.* 10(2):189–221, 2012.

[12]Cho, Y., W. Lee, E.-A. Park, I.-Y. Oh, E.-K. Choi, J.-W. Seo, *et al*. The anatomical characteristics of three different endocardial lines in the left atrium: evaluation by computed tomography prior to mitral isthmus block attempt. *Europace* 14:1104–1111, 2012. doi:10.1093/europace/eus051.

[13]Cochet, H., D. Scherr, S. Zellerhoff, F. Sacher, N. Derval, A. Denis, *et al*. Atrial structure and function 5 years after successful ablation for persistent atrial fibrillation: an MRI study. *J. Cardiovasc. Electrophysiol.* 25:671–679, 2014. doi:10.1111/jce.12449.

[14]Colli Franzone, P., L. F. Pavarino, and S. Scacchi. Mathematical Cardiac Electrophysiology, Vol. 13. Cham: Springer International Publishing, 2014.

[15]Corrado, C., J.-F. Gerbeau, and P. Moreau. Identification of weakly coupled multiphysics problems. Application to the inverse problem of electrocardiography. *J. Comput. Phys.* 283:271–298, 2015. doi:10.1016/j.jcp.2014.11.041.

[16]De Ponti, R., S. Y. Ho, J. A. Salerno-Uriarte, M. Tritto, and G. Spadacini. Electroanatomic analysis of sinus impulse propagation in normal human atria. *J. Cardiovasc. Electrophysiol.* 13:1–10, 2002. doi:10.1046/j.1540-8167.2002.00001.x.

[17]Geuzaine, C., and J.-F. Remacle. Gmsh: a 3-D finite element mesh generator with built-in pre-and post-processing facilities. *Int. J. Numer. Methods Eng.* 79:1309–1331, 2009.

[18]Haissaguerre, M., M. Hocini, A. Denis, A. J. Shah, Y. Komatsu, S. Yamashita, *et al*. Driver domains in persistent

atrial fibrillation. *Circulation* 130:530–538, 2014. doi: 10.1161/CIRCULATIONAHA.113.005421.

[19]Haïssaguerre, M., P. Jaïs, D. C. Shah, A. Takahashi, M. Hocini, G. Quiniou, *et al.* Spontaneous initiation of atrial fibrillation by ectopic beats originating in the pulmonary veins. *N. Engl. J. Med.* 339:659–666, 1998. doi: 10.1056/NEJM199809033391003.

[20]Heeringa, J., D. A. M. van der Kuip, A. Hofman, J. A. Kors, G. van Herpen, B. H. C. Stricker, *et al.* Prevalence, incidence and lifetime risk of atrial fibrillation: the Rotterdam study. *Eur. Heart J.* 27:949–953, 2006. doi: 10.1093/eurheartj/ehi825.

[21]Ho, S. Y., R. H. Anderson, and D. Sánchez-Quintana. Atrial structure and fibres: morphologic bases of atrial conduction. *Cardiovasc. Res.* 54:325–336, 2002. doi: 10.1016/S0008-6363(02)00226-2.

[22]Hoermann, J. M., C. Bertoglio, and W. A. Wall. Discontinuous approximations for electrophysiology problems. In: 4th International Conference on Computational and Mathematical Biomedical Engineering, 2015, pp. 692–695.

[23]Huemer, M., A. Wutzler, A. S. Parwani, P. Attanasio, H. Matsuda, F. Blaschke, *et al.* Comparison of the anterior and posterior mitral isthmus ablation lines in patients with perimitral annulus flutter or persistent atrial fibrillation. *J. Interv. Cardiac Electrophysiol.* 44:119–129, 2015. doi: 10.1007/s10840-015-0033-1.

[24]Krahn, A. D., J. Manfreda, R. B. Tate, F. A. L. Mathewson, and T. E. Cuddy. The natural history of atrial fibrillation: incidence, risk factors, and prognosis in the manitoba follow-up study. *Am. J. Med.* 98:476–484, 1995. doi:10.1016/S0002-9343(99)80348-9.

[25]Krogh-Madsen, T., G. W. Abbott, and D. J. Christini. Effects of electrical and structural remodeling on atrial fibrillation maintenance: A simulation study. *PLoS Comput. Biol.* 2012. doi:10.1371/journal.pcbi.1002390.

[26]Krueger, M. W., W. H. W. Schulze, K. S. Rhode, R. Razavi, G. Seemann, and O. Dössel. Towards personalized clinical in silico modeling of atrial anatomy and electrophysiology. *Med. Biol. Eng. Comput.* 51:1251–1260, 2013. doi:10.1007/s11517-012-0970-0.

[27]Krueger, M. W., G. Seemann, K. Rhode, D. U. J. Keller, C. Schilling, A. Arujuna, *et al.* Personalization of atrial anatomy and electrophysiology as a basis for clinical modeling of radio-frequency ablation of atrial fibrillation. *IEEE Trans. Med. Imaging* 32:73–84, 2013. doi: 10.1109/TMI.2012.2201948.

[28]Lemery, R., L. Soucie, B. Martin, A. S. L. Tang, M. Green, and J. Healey. Human study of biatrial electrical coupling determinants of endocardial septal activation and conduction over interatrial connections. *Circulation* 110:2083–2089, 2004. doi:10.1161/01.CIR.0000144461.83835.A1.

[29]Moireau, P., C. Bertoglio, N. Xiao, C. A. Figueroa, C. A. Taylor, D. Chapelle, *et al.* Sequential identification of boundary support parameters in a fluid–structure vascular model using patient image data. *Biomech. Model. Mechanobiol.* 12:475–496, 2012. doi:10.1007/s10237-012-0418-3.

[30]Nagler, A., C. Bertoglio, C. T. Stoeck, S. Kozerke, and W. A. Wall. Cardiac fibers estimation from arbitrarily spaced diffusion weighted MRI. In: Functional Imaging and Modeling of the Heart, edited by H. van Assen, P. Bovendeerd, and T. Delhaas. Springer International Publishing, 2015, pp. 198–206. doi:10.1007/978-3-319-20309-6_23.

[31]Nagler, A., C. Bertoglio, M. Gee, and W. Wall. Personalization of cardiac fiber orientations from image data using the unscented kalman filter. In: Funct. Imaging Model. Heart, edited by S. Ourselin, D. Rueckert, and N. Smith. Berlin: Springer, 2013, pp. 132–140.

[32]Reumann, M., J. Bohnert, G. Seemann, B. Osswald, and O. Dossel. Preventive ablation strategies in a biophysical model of atrial fibrillation based on realistic anatomical data. *IEEE Trans. Biomed. Eng.* 55:399–406, 2008. doi: 10.1109/TBME.2007.912672.

[33]Rotter, M., L. Dang, V. Jacquemet, N. Virag, L. Kappenberger, and M. Haïssaguerre. Impact of varying ablation patterns in a simulation model of persistent atrial fibrillation. *Pacing Clin. Electrophysiol.* 30:314–321, 2007. doi:10.1111/j.1540-8159.2007.00671.x.

[34]Sanders, P., P. Jaïs, M. Hocini, L.-F. Hsu, C. Scavée, F. Sacher, *et al.* Electrophysiologic and clinical consequences of linear catheter ablation to transect the anterior left atrium in patients with atrial fibrillation. *Heart Rhythm* 1:176–184, 2004. doi:10.1016/j.hrthm.2004.03.072.

[35]Schotten, U., S. Verheule, P. Kirchhof, and A. Goette. Pathophysiological mechanisms of atrial fibrillation: a translational appraisal. *Physiol. Rev.* 91:265–325, 2011. doi: 10.1152/physrev.00031.2009.

[36]Shah, A. J., M. Hocini, O. Xhaet, P. Pascale, L. Roten, S. B. Wilton, *et al.* Validation of novel 3-dimensional electrocardiographic mapping of atrial tachycardias by invasive mapping and ablation: a multicenter study. *J. Am. Coll. Cardiol.* 62:889–897, 2013. doi:10.1016/j.jacc.2013.03.082.

[37]Shi, Y., P. Lawford, and R. Hose. Review of zero-D and 1-D models of blood flow in the cardiovascular system. *Biomed. Eng. OnLine* 10:33, 2011. doi:10.1186/1475-925X-10-33.

[38]Sparks, P. B., H. G. Mond, J. K. Vohra, S. Jayaprakash, and J. M. Kalman. Electrical remodeling of the atria following loss of atrioventricular synchrony. A long-term study in humans. *Circulation* 100:1894–1900, 1999. doi: 10.1161/01.CIR.100.18.1894.

[39]Sparks, P. B., H. G. Mond, J. K. Vohra, A. G. Yapanis, L. E. Grigg, and J. M. Kalman. Mechanical remodeling of the left atrium after loss of atrioventricular synchrony a long-term study in humans. *Circulation* 100:1714–1721, 1999. doi:10.1161/01.CIR.100.16.1714.

[40]Verma, A., C. Jiang, T. R. Betts, J. Chen, I. Deisenhofer, R. Mantovan, *et al.* Approaches to catheter ablation for persistent atrial fibrillation. *N. Engl. J. Med.* 372:1812–1822, 2015. doi:10.1056/NEJMoa1408288.

[41]Weber, F. M., S. Lurz, D. U. J. Keller, D. L. Weiss, G. Seemann, C. Lorenz, *et al.* Adaptation of a minimal four-state cell model for reproducing atrial excitation properties. *Comput. Cardiol.* 2008:61–64, 2008. doi:10.1109/CIC.2008.4748977.

[42]Wolf, P. A., R. D. Abbott, and W. B. Kannel. Atrial fibrillation as an independent risk factor for stroke: the Framingham study. *Stroke* 22:983–988, 1991. doi: 10.1161/01.STR.22.8.983.